# Vibrational Assignments of Two Polymorphic Forms of Metaxolone by Using DFT Calculations and the SQM Methodology

**Maximiliano A. Iramain[1], Maria J. Márquez[1], Ana E. Ledesma[2], Silvia Antonia Brandán[1,*]**

[1]*Cátedra de Química General, Instituto de Química Inorgánica, Facultad de Bioquímica. Química y Farmacia, Universidad Nacional de Tucumán, Ayacucho 471, (4000) San Miguel de Tucumán, Tucumán, Argentina.*

[2]*Cátedra de Química, Departamento Académico de Química, Facultad de Ciencias Exactas y Tecnologías, Universidad Nacional de Santiago del Estero, CONICET, Av. Belgrano Sur 1912, (4200) Santiago del Estero, Argentina.*

**ABSTRACT**

A theoretical study has been performed on the muscle relaxant 5-[(3, 5-dimethylphenoxy)methyl]-1,3-oxazolidin-2-one, of generic name metaxolone (MTX), by using the hybrid B3LYP/6-31G calculations in the gas phase and the experimental available infrared and Raman spectra in the solid phase. Three *C1,* C2 and *C3* isomers were found in the potential energy surface (PES) but only two of them, *C1* and *C2* correspond to those experimentally reported polymorphic forms A and B, respectively. The absence of *C3* isomer could be easily explained by the quite high values in the dihedral C5-C7-O2-C9 and O1-C5-C7-O2 angles different from those experimental structures reported for the two polymorphic forms A and B of MTX. On the other hand, the higher bond orders values together with the high topological properties observed for the oxazolidinone ring of *C1* could possibly support their existence despite this isomer has highest energy than *C2* and *C3*. The natural bond orbital (NBO) analyses reveal the high stabilities of *C1* and *C2* while the atoms in molecules(AIM) study suggests that the ring dimethylphenoxy-methyl practically do not have influence on the properties of MTX. The frontier orbitals show that the isomers of MTX have reactivities and electrophilicity indexes similar to antiviral thymidine while their nucleophilicity indexes present values closer to antimicrobial thione. In addition, the complete vibrational assignments of those two stable isomers were performed by using the experimental available FT-IR and FT-Raman spectra, their normal internal coordinates,the scaled quantum mechanical force field (SQMFF) methodology and the Molvib program.The harmonic force fields for the two isomers and their corresponding force constants were also reported. The force constants values are in agreement with values reported in the literature for species with similar groups.

## 1.INTRODUCTION

Metaxolone is the generic name of a drug, known from long time ago, that structurally is an oxazolidinone specie named 5-[(3,5-dimethylphenoxy)methyl]-1,3-oxazolidin-2-one [1-12]. This drug presents therapeutic properties because act on centrally acting skeletal muscle relaxant [2] although it also has many contraindications with various difficult cases reported in the literature [13-15]. The insolubility of this drug in water is a great problem and, for this reason, metaxolone is normally combined in pharmaceutical preparations with others, such as diclofenac to improve their incorporation maintain the effects and properties of their active ingredients [6-8,10,11]. However, during the design of these preparations the physicochemical properties of the ingredients and their activities can be modified. In fact, pharmaceutical cocrystals can be employed to improve their physicochemical characteristics maintaining its therapeutic properties [16, 17]. Hence, few methods and techniques are reported in the literature to determine the compositions and dosage of these preparations, as reported by Patel et al. [8], therefore, common spectroscopic techniques are employed for these purposes [9,12,16]. Chattopadhyay et al. [1] and Lorimer et al. [3] have reported the FT-IR and FT-Raman spectra of two polymorphic forms of metaxolone while Aitipamula et al. [4] have performed an experimental conformational study of both structures showing that the form B is thermodynamically the most stable form at ambient conditions. On the other hand, Lin et al. [5] have studied the cocrystal formation of metaxolone with short-chain dicarboxylic acids while Boopathi et al.[12] have recently reported a spectroscopic study on metaxolone by using the FT-IR, FT-Raman, and NMR spectra and DFT calculations. However, in this study, the two experimental polymorphic forms of this drug were not considered and only 54 vibration modes of a total of 87 were assigned only by using scale factors and the B3LYP/6-311++G** calculations [12], with this scenario, the vibrational studies of both forms of metaxolone are of interest to characterize completely both forms by using their experimental FT-IR and FT-Raman spectra. The identification of both forms is necessary and useful in all pharmaceutical preparations, as mentioned above. Taking into account this purpose, we have carried out the theoretical conformational study of metaxolone, indispensable to know which is the most stable structure, in order to perform the complete vibrational assignments of the experimental available vibrational spectra of metaxolone by using the scaled quantum mechanical force field (SQMFF) procedure [18] and the Molvib program [19]. Here, calculations based on the density functional theory (DFT) with the hybrid B3LYP method were used to optimize the two initial structures of metaxolone by

*Citation: Silvia Antonia Brandán et al. Ijsrm.Human, 2018; Vol. 8 (3): 312-334.*

313

using the 6-31G* basis set [20,21]. Here, it is necessary to explain that the calculations were performed with the B3LYP/6-31G* method because with the greater basis set the studies were already reported [12], as mentioned before. Additional calculations by using the NBO and AIM2000 programs were performed in order to search the importance of the oxazolidinone rings of both forms on the dimethylphenoxy-methyl ones [22-24]. Besides, the predictions of the reactivities of both forms are very important to explain their biological activities and kinetics properties, especially because now the mechanisms to explain the therapeutic properties of this muscle relaxant remain unknown. Thus, the frontier orbitals [24,25] and some descriptors were calculated by using the same level of theory [26-30]. Here, these properties obtained for metaxolone were later compared with those studied by Boopathi et al. [12] by using B3LYP/6-311++G** calculations and with other compounds containing different rings in their structures and different biological activities [31-33].

## 2. COMPUTATIONAL DETAILS

Both forms of metaxolone (MTX) were modeled with the *GaussView* program [34] and optimized by using the hybrid B3LYP/6-31G* method with the Gaussian 09program [35]. Later, the potential energy surfaces (PES) were studied for variations of the dihedral C5-C7-O2-C9 and O1-C5-C7-O2 angles by using the same level of theory where, in particular for the curve in function of the O1-C5-C7-O2 angle clearly shows three theoretical structures, two of them with local minima and one with a global minimum, as expected. These structures are named *C1*, *C2*, and *C3*; being *C2* the most structure corresponding to a global minimum while*C1* is the less stable with a higher energy value than *C2* and *C3*. In Figure 1 are presented the three theoretical structures of metaxolone in the gas phase by using the B3LYP/6-31G* level of theory. Here, all properties were presented for the three structures in order to explain the differences among the three isomers. The atomic natural populations (NPA) and MK (Merz-Kollman) charges and the molecular electrostatic potentials (MEP) were computed in the gas phase at the same level of the theory [22,36]. NBO calculations [19] were also performed to calculate the bond orders, expressed as Wiberg indexes, and the acceptor-donor interactions energies while the AIM2000 program [20] was used to compute the topological properties of all isomers of MTX. Here, the harmonic force fields were also calculated by using the corresponding normal internal coordinates together with the SQMFF methodology [18] and the Molvib program [19].

*Citation: Silvia Antonia Brandán et al. Ijsrm.Human, 2018; Vol. 8 (3): 312-334.*

314
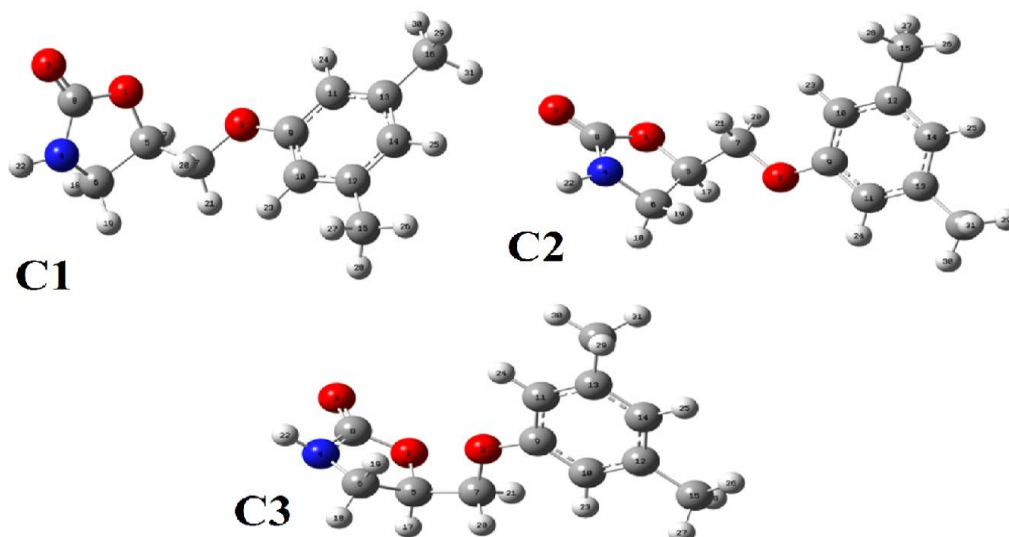
**Figure 1:Molecular theoretical structures of metaxolone and the atoms numbering by using the B3LYP/6-31G\* method.**

To perform the vibrational assignments for those two isomers only those Potential Energy Distribution (PED) contributions ≥ 10% were considered. Thus, the predicted IR and Raman for the isomers of MTX were compared with those experimental available for MTX [1,3,12]. The root-mean-square deviation (RMSD) was employed to compare the theoretical and experimental results of geometries in order to know the differences between these values for all isomers of MTX. The volumes in the gas phase were calculated with the Moldraw program [37] while the differences between their frontier orbitals, known as the gap, and some global descriptors were also computed in order to know their reactivity's and behaviors [27-30]. Then, these results for the three isomers were exhaustively compared and analyzed between them.

## 3. RESULTS AND DISCUSSION

### 3.1. Geometries in gas phase

The results from the conformational studies for MTX can be seen in **Table 1**. The calculated total and relative energies, dipole moments, volume values and populations are presented in that table for the three most stable conformers by using the B3LYP/6-31G\* method. Regarding the values of Table 1, it is observed that *C2* is the most stable conformer of MTX with higher volume and population but with the lowest dipole moment value than *C1* and *C3*. Note that the higher relative energy for *C1* generates a lower population. Despite the low

*Citation: Silvia Antonia Brandán et al. Ijsrm.Human, 2018; Vol. 8 (3): 312-334.*

315

energy value observed for *C1*, this isomer exists in the solid phase because their high dipole moment value probably stabilizes this species, as we see later.

**Table 1. Calculated total (*E*) and relative energies (Δ*E*), dipolar moment (μ), volume (V) and population values for the most stable conformers of 5-[(3,5 dimethylphenoxy)methyl]-1,3-oxazolidin-2-one in the gas phase.**

| B3LYP/6-31G*method/Gas phase | | | | | |
|---|---|---|---|---|---|
| Conformers | *E* (Hartrees) | Δ*E* (kJ/mol) | μ(Debye) | V (Å$^3$) | Population |
| *C1* | -746.7484 | 8.66 | 5.36 | 242.8 | 2.30 |
| *C2* | -746.7517 | 0.00 | 4.22 | 245.9 | 76.33 |
| *C3* | -746.7505 | 3.15 | 5.36 | 242.5 | 21.37 |

The geometrical parameters for *C1*, *C2*, and *C3* were compared in **Table 2** with those experimental reported for both polymeric A and B forms by Aitipamula et al. [4] by means of the RMSD values, which are also presented in bold letter in Table 2. The deep analyses of the values show interesting results. Firstly, it is observed that the predicted C8=O3, C5-O1, C7-O2 and C9-O2 distances present lower values than the experimental ones while a contrary relationship is observed for the C8-O1, N4-C6 and N4-C8 distances. In particular, the experimental O1---O2 distance for the form A is similar to that predicted for the *C1* and *C3* isomers while for *C2* that predicted distance is similar to the experimental determined for the form B. Then, the RMSD values (0.021-0.019 Å) for the three isomers present practically identical values when they are compared with both forms A and B, being slightly lower for the most stable isomer *C2*. When the bond angles for *C1*, *C2* and *C3* are analyzed similar RMSD values (1.8-1.4 º) are obtained, wherein particular, it is observed that the bond N4-C6-C5 angles practically have the same values than those experimentally observed for the forms A and B. Here, some bond angles are predicted over-dimensioned, as observed in the bond lengths. The higher variations are observed in the dihedral angles with RMSD values between 258 and 5.3 º. Here, it is observed that the *C2* isomer presents values and signs similar to the experimental form B, hence, this isomer presents the lowest value than *C1* and *C3* (5.3 º) while the *C1* isomer have lowest RMSD value of dihedral angles and signs similar to the experimental form A. Later, these analyses show clearly that the structures of both *C1* and *C2* isomers correspond to those polymorphic forms found experimentally for MTX (A and B) by different authors [1,3,4], as observed in **Figure 2.**

*Citation: Silvia Antonia Brandán et al. Ijsrm.Human, 2018; Vol. 8 (3): 312-334.*

316

**Table 2. Calculated geometrical parameters for 5-[(3,5-dimethylphenoxy)methyl]-1,3-oxazolidin-2-one compared with the experimental ones for the A and B forms.**

| Parameters | B3LYP/6-31G* Method[a] | | | Experimental[b] | |
|---|---|---|---|---|---|
| | *C1* | *C2* | *C3* | A Form | B Form |
| Bond lengths (Å) | | | | | |
| C8=O3 | 1.204 | 1.204 | 1.204 | 1.226 | 1.226 |
| C5-O1 | 1.439 | 1.438 | 1.437 | 1.463 | 1.459 |
| C8-O1 | 1.372 | 1.377 | 1.373 | 1.361 | 1.364 |
| C7-O2 | 1.413 | 1.419 | 1.414 | 1.430 | 1.431 |
| C9-O2 | 1.371 | 1.373 | 1.372 | 1.372 | 1.377 |
| N4-C6 | 1.450 | 1.453 | 1.453 | 1.454 | 1.445 |
| N4-C8 | 1.383 | 1.379 | 1.381 | 1.338 | 1.336 |
| C5-C6 | 1.548 | 1.544 | 1.546 | 1.525 | 1.530 |
| O1-O2 | 2.865 | 3.619 | 2.883 | 2.888 | 3.621 |
| **RMSD A** | **0.021** | **0.020** | **0.021** | | |
| **RMSD B** | **0.021** | **0.019** | **0.020** | | |
| Bond angles (º) | | | | | |
| C5-O1-C8 | 110.2 | 109.8 | 110.1 | 107.7 | 108.0 |
| O1-C8-N4 | 108.1 | 107.9 | 108.1 | 110.2 | 110.2 |
| C8-N4-C6 | 111.4 | 111.5 | 111.3 | 111.5 | 112.4 |
| N4-C6-C5 | 100.1 | 99.8 | 100.0 | 99.9 | 100.7 |
| C6-C5-O1 | 104.5 | 104.6 | 104.7 | 103.8 | 104.5 |
| C5-C7-O2 | 107.6 | 106.4 | 108.7 | 107.5 | 105.9 |
| C7-O2-C9 | 118.6 | 118.7 | 118.7 | 117.2 | 116.4 |
| **RMSD A** | **1.4** | **1.4** | **1.5** | | |
| **RMSD B** | **1.6** | **1.5** | **1.8** | | |
| Dihedral angles (º) | | | | | |
| O1-C5-C7-O2 | -66.5 | -176.0 | 67.4 | -69.8 | -179.0 |
| C5-C7-O2-C9 | 177.5 | -179.3 | -178.5 | 167.6 | -169.3 |
| C9-C10-C12- | 179.7 | -179.8 | -179.4 | 178.2 | -178.6 |
| C9-C11-C13- | -179.6 | -179.9 | -179.6 | -179.0 | -179.4 |
| **RMSD A** | **5.3** | **254.8** | **258.1** | | |
| **RMSD B** | **255.6** | **5.3** | **123.3** | | |

[a]This work; from Ref. [4]; RMSD, in bold letter.

The distances between the two electronegative O atoms (O1---O2) could not justify the not existence of *C3* because their value is similar to that observed for the experimental form A. Here, the higher discrepancies observed in the RMSD values of the dihedral angles (258.1 and 123.3 º) could probably explain in part the absence of *C3* isomer in the gas phase and hence, in the solid phase. These comparisons between theoretical and experimental studies suggest clearly that only the two *C1* and *C2* isomers should be considered in the vibrational analysis.

*Citation: Silvia Antonia Brandán et al. Ijsrm.Human, 2018; Vol. 8 (3): 312-334.*

317
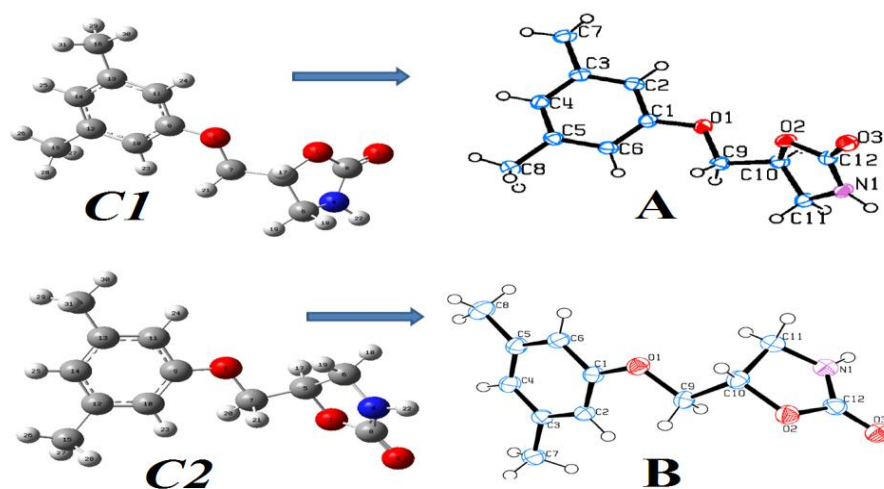
**Figure 2. Comparisons between the theoretical structures for the isomer *C1* and *C2* with the corresponding polymeric experimental ones A and B, respectively from Ref [4].**

### 3.2. NPA and MK Charges, MEP and BO studies

Here, it is very important to justify the existence of *C1* despite of their low energy value and, also, the absence of *C3*. For these reasons, the atomic natural populations (NPA) and Merz-Kollman (MK) charges [36] were studied together with the molecular electrostatic potential (MEP). Besides, the bond order expressed as Wiberg indexes were also calculated by using the NBO program [22] because these parameters could show some important differences. Table 3 shows those three properties calculated for the three isomers of MTX in the gas phase.

**Table 3. Calculated MK and NPA charges and the MEP values for the most stable conformers of 5-[(3,5-dimethylphenoxy)methyl]-1,3-oxazolidin-2-one.**

| B3LYP/6-31G* Method | | | | | | | | |
|---|---|---|---|---|---|---|---|---|
| | MK charges | | | NPA charges | | | MEP | | |
| Atoms | *C1* | *C2* | *C3* | *C1* | *C2* | *C3* | *C1* | *C2* | *C3* |
| 1 O | -0.348 | -0.425 | -0.377 | -0.552 | -0.562 | -0.559 | -22.276 | -22.273 | -22.279 |
| 2 O | -0.281 | -0.495 | -0.235 | -0.528 | -0.544 | -0.538 | -22.281 | -22.274 | -22.275 |
| 3 O | -0.529 | -0.525 | -0.522 | -0.606 | -0.607 | -0.609 | -22.347 | -22.346 | -22.351 |
| 4 N | -0.650 | -0.622 | -0.707 | -0.708 | -0.706 | -0.704 | -18.308 | -18.309 | -18.315 |
| 5 C | 0.020 | 0.205 | 0.155 | 0.063 | 0.070 | 0.062 | -14.655 | -14.657 | -14.655 |
| 6 C | 0.208 | 0.160 | 0.300 | -0.283 | -0.285 | -0.284 | -14.671 | -14.679 | -14.681 |
| 7 C | 0.060 | 0.156 | -0.116 | -0.129 | -0.130 | -0.126 | -14.668 | -14.670 | -14.664 |
| 8 C | 0.762 | 0.751 | 0.756 | 0.931 | 0.930 | 0.936 | -14.593 | -14.592 | -14.597 |
| 9 C | 0.473 | 0.705 | 0.452 | 0.332 | 0.330 | 0.332 | -14.682 | -14.677 | -14.678 |

*Citation: Silvia Antonia Brandán et al. Ijsrm.Human, 2018; Vol. 8 (3): 312-334.*

318

The dihedral angles involved in the oxazolidinone rings of the different isomers have suggested differences among them and, hence, only the values for the atoms involved in their rings are reported in Table 3. Analyzing deeply these results it is observed that the MK charges values are very different to the NPA charges and, apparently, there are not differences among the values for the three isomers but, when the MK charges are represented in function of their atoms we can see clearly these differences. Thus, **Figure 3** shows the MK charges taking into account the involved atoms. The graphic shows that the MK charge on the O2 atom corresponding to *C2* present the lowest value than *C1* and *C3* while the charges on the C7 and C9 atoms for this isomer have higher values than those observed on the other two isomers. Evidently, these results explain the stability of *C2* because the distance between the two O1 and O2 atoms is longer than *C1* and *C3*, as observed in Table 2.
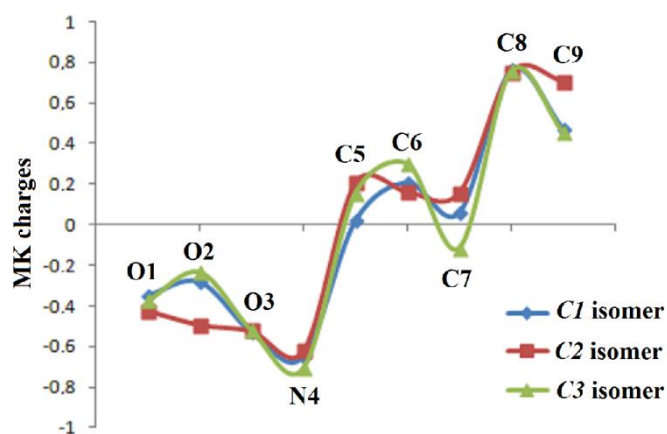


**Figure 3**. **Calculated MK charges on the atoms corresponding to the most stable isomers of 5-[(3,5-dimethylphenoxy)methyl]-1,3-oxazolidin-2-one in the gas phase by using the B3LYP/6-31G\* Method.**

Then, in *C3* it is observed the lower negative MK value on the C7 atom and the most positive value on the C9 atom. Hence, probably these different values could explain the differences in the dihedral C5-C7-O2-C9 and O1-C5-C7-O2 angles and, in particular, in the value of 67.4 ° predicted for theO1-C5-C7-O2 angle of *C3*. When the NPA charges on those atoms are analyzed for the three isomers we observed the same behaviors in the three isomers and, in particular, the higher positive values are observed on the C5 and C8 atoms while the less negative values are observed on the N4 atoms. Obviously, on the three O atoms are observed negative NPA charges but slightly higher than those observed on the N4 atoms. These NPA charges do not show differences among the isomers.

*Citation: Silvia Antonia Brandán et al. Ijsrm.Human, 2018; Vol. 8 (3): 312-334.*

319

The deep analysis of the MEP values only show the differences on the atoms due to their electronegativities, as expected, thus, the less negative values are observed on the C atoms while the most negative values on the O atoms showing the following tendency: C < N < O. The mapped MEP surfaces are observed for the three isomers in **Figure 4** where we can see red colours on the O1, O2 and O3 atoms and the blue colours on the H atoms belong to the N-H groups. Probably, the higher MEP values observed on the O3 atoms from Table 3 for the *C1* and *C3* isomers could justify the differences observed in the colorations on the dimethylphenoxy-methyl rings.
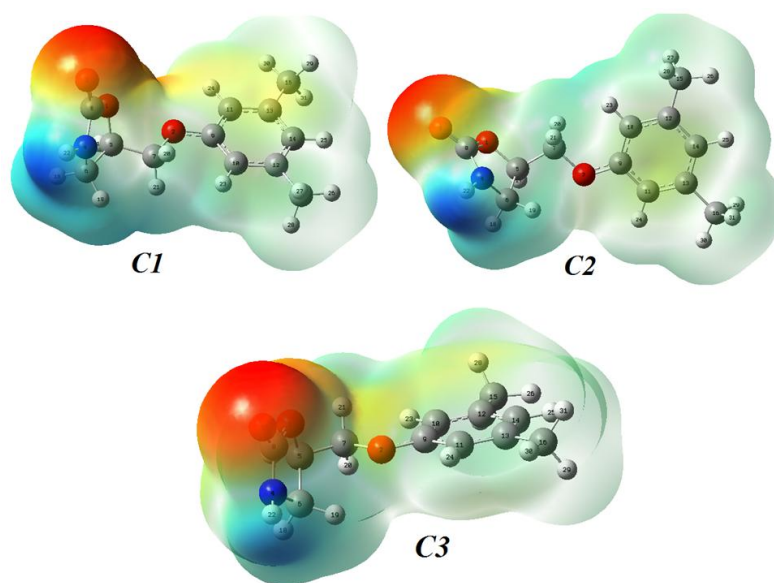


**Figure 4**. **Calculated electrostatic potential surfaces on the molecular surface ofthe most stable isomers of 5-[(3,5-dimethylphenoxy)methyl]-1,3-oxazolidin-2-one in the gas phase. Color ranges, in au: from red -0.090 to blue +0.090. B3LYP functional and 6-31G\* basis set. Isodensity value of 0.005.**

The red colors are characteristics of nucleophilic sites while the blue colors of electrophilic sites. Evidently, these two reactive regions are located on the oxazolidinone rings while the dimethylphenoxy-methyl rings are practically inert sites.

The bond orders (BO) for the three isomers of MTX are summarized in**Table 4.**

*Citation: Silvia Antonia Brandán et al. Ijsrm.Human, 2018; Vol. 8 (3): 312-334.*

320

**Table 4. Calculated bond orders expressed, as Wiberg indexes by atoms, for the three isomers of 5-[(3,5-dimethylphenoxy)methyl]-1,3-oxazolidin-2-one.**

| | B3LYP/6-31G* Method | | |
|---|---|---|---|
| Atoms | *C1* | *C2* | *C3* |
| 1 O | 2.113 | 2.099 | 2.106 |
| 2 O | 2.120 | 2.102 | 2.112 |
| 3 O | 2.040 | 2.039 | 2.036 |
| 4 N | 3.097 | 3.105 | 3.100 |
| 5 C | 3.849 | 3.844 | 3.856 |
| 6 C | 3.851 | 3.844 | 3.846 |
| 7 C | 3.800 | 3.788 | 3.792 |
| 8 C | 3.835 | 3.835 | 3.831 |
| 9 C | 3.903 | 3.901 | 3.901 |

Evaluating, these BO values we observed that in the *C1* isomer the three O atoms and the C6, C7 and C9 atoms have slightly higher values than the corresponding to the other two isomers this observation probably could explain in part their existence due to their higher stability while in the *C3* isomer only the C5 atom present a higher value than the other ones. On the other hand, the N4 atom in *C2* presents slightly higher value than the other two isomers. This way, this study possibly supports the existence of the *C1* isomer despite their high-energy value.

### 3.3. NBO and AIM studies

The donor-acceptor energy interactions and the topological properties are important parameters that can predict the stabilities of these three isomers of MTX due to the presence of O and N atoms with lone pairs and different rings in their structures. Hence, the charge transfers can be investigated with the NBO program [22] while the intra-molecular interactions can be easily explained by using the Bader' theory [24] and the AIM2000 program [23]. In **Table 5** are presented the second order perturbation theory analysis of Fock matrix in NBO Basis calculated from the NBO calculations. Five different $\Delta ET_{\pi \to \pi^*}$, $\Delta ET_{LP \to \pi^*}$, $\Delta ET_{\sigma^* \to \pi^*}$, $\Delta ET_{LP \to \sigma^*}$ and $\Delta ET_{\pi^* \to \pi^*}$ interactions from lone pairs of the O and N atoms (LP) or different orbital toward different $\sigma$ or $\pi$ C-C, O-C or N-C orbitals are observed in Table 5 for the three isomers and, these results clearly show that the $\Delta ET_{\pi^* \to \pi^*}$ interactions present the higher values. Then, the total donor-acceptor energy interactions support mainly to the *C2* and *C1* isomers although the *C3* isomer also shows a great stability in the gas phase. The results obtained from the AIM calculations are presented in **Table 6**.

*Citation: Silvia Antonia Brandán et al. Ijsrm.Human, 2018; Vol. 8 (3): 312-334.*

321

**Table 5. Main donor-acceptor energy interactions (in kJ/mol) for the three isomers of 5-[(3,5-dimethylphenoxy)methyl]-1,3-oxazolidin-2-one.**

| B3LYP/6-31G* | | | |
|---|---|---|---|
| Delocalization | *C1* | *C2* | *C3* |
| $\pi C9\text{-}C10 \rightarrow \pi^*C11\text{-}C13$ | 62.52 | 63.19 | 62.69 |
| $\pi C9\text{-}C10 \rightarrow \pi^*C12\text{-}C14$ | 91.56 | 91.15 | 91.19 |
| $\pi\, C11\text{-}C13 \rightarrow \pi^*\, C9\text{-}C10$ | 97.51 | 97.30 | 97.80 |
| $\pi\, C11\text{-}C13 \rightarrow \pi^*\, C12\text{-}C14$ | 66.56 | 65.89 | 66.44 |
| $\pi\, C12\text{-}C14 \rightarrow \pi^*\, C9\text{-}C10$ | 66.56 | 67.31 | 67.06 |
| $\pi\, C12\text{-}C14 \rightarrow \pi^*\, C11\text{-}C13$ | 94.93 | 96.30 | 95.56 |
| $\boldsymbol{\Delta ET_{\pi \rightarrow \pi^*}}$ | **479.65** | **481.15** | **480.73** |
| $LPO2 \rightarrow \pi^*\, C9\text{-}C10$ | 121.93 | 118.60 | 119.89 |
| $\boldsymbol{\Delta ET_{LP \rightarrow \pi^*}}$ | **121.93** | **118.60** | **119.89** |
| $\sigma^*O3\text{-}C8 \rightarrow \pi^*O3\text{-}C8$ | 129.88 | 109.78 | 82.78 |
| $\boldsymbol{\Delta ET_{\sigma+ \rightarrow \pi^*}}$ | **129.88** | **109.78** | **82.78** |
| $LPO1 \rightarrow \sigma^*O3\text{-}C8$ | 104.17 | 105.33 | 118.06 |
| $LPO3 \rightarrow \sigma^*O1\text{-}C8$ | 148.51 | 151.17 | 149.47 |
| $LPO3 \rightarrow \sigma^*N4\text{-}C8$ | 106.70 | 104.67 | 105.29 |
| $LPN4 \rightarrow \sigma^*\, O3\text{-}C8$ | 133.95 | 148.55 | 152.55 |
| $\boldsymbol{\Delta ET_{LP \rightarrow \sigma^*}}$ | **493.33** | **509.72** | **525.37** |
| $\pi^*\, C9\text{-}C10 \rightarrow \pi^*\, C11\text{-}C13$ | 763.61 | 850.84 | 770.76 |
| $\pi^*\, C9\text{-}C10 \rightarrow \pi^*\, C12\text{-}C14$ | 770.14 | 761.11 | 743.85 |
| $\boldsymbol{\Delta ET_{\pi^* \rightarrow \pi^*}}$ | **1533.75** | **1611.96** | **1514.61** |
| $\boldsymbol{\Delta E_{Total}}$ | **2758.54** | **2831.21** | **2723.38** |

Here, only the electron density, $\rho(r)$ and the Laplacian values, $\Box^2\rho(r)$ were computed for the three isomers in the ring critical points (RCPs) of both oxazolidinone and dimethylphenoxy-methyl rings because there are not observed intra-molecular interactions.

**Table 6. Analysis of the topological properties of the three isomers of 5-[(3,5-dimethylphenoxy)methyl]-1,3-oxazolidin-2-one in the gas phase.**

| B3LYP/6-31G* | | | | | | |
|---|---|---|---|---|---|---|
| Parameter | Oxazolidinone ring | | | Dimethylphenoxy-methyl ring | | |
| (a.u.) | *C1* | *C2* | *C3* | *C1* | *C2* | *C3* |
| $\rho(r_c)$ | 0.04192 | 0.04217 | 0.04191 | 0.01974 | 0.01975 | 0.01974 |
| $\nabla^2\rho(r_c)$ | 0.3286 | 0.3298 | 0.3281 | 0.1572 | 0.1572 | 0.1572 |

The exhaustive analyses from the data show that the properties corresponding to the dimethylphenoxy-methyl rings in the three isomers practically do not change and only important changes are observed in the oxazolidinone rings. Thus, as suggested initially the properties corresponding to the atoms belonging to these oxazolidinone rings were considered. A very important result it is observed for those two topological properties

*Citation: Silvia Antonia Brandán et al. Ijsrm.Human, 2018; Vol. 8 (3): 312-334.*

322

presented in the RCP corresponding to the *C2* isomer because these have the highest values than *C1* and *C3* while the lower values are observed for *C3*. Hence, this result could partially explain the presence of *C1* in the gas phase and, hence, also probably their existence in the solid state.

### 3.5. Frontier orbitals and global descriptors

For the three isomers of MTX is very important to predict the reactivities and behaviors taking into account that MTX is used as a drug with skeletal muscle relaxant properties. Hence, the frontier orbitals were used to calculate the gap values [25,26] and, then, to compute some interesting descriptors by using known equations [27-31]. The results were presented in **Table 7** compared with those reported for MTX by using the 6-311++G** basis set [12].

**Table 7. Calculated HOMO and LUMO orbitals, energy band gap, chemical potential ($\mu$), electronegativity ($\chi$), global hardness ($\eta$), global softness ($S$), global electrophilicity index ($\omega$) and global nucleophilicity index ($E$) for the three isomers of 5-[(3,5-dimethylphenoxy)methyl]-1,3-oxazolidin-2-one in gas phase.**

| Frontier orbitals | B3LYP/6-31G* method[s] | | | B3LYP/6-311++G**[b] |
|---|---|---|---|---|
| | *C1* | *C2* | *C3* | |
| HOMO | -5.8704 | -5.9947 | -5.9739 | -6.3810 |
| LUMO | 0.1174 | 0.0100 | 0.0245 | -0.5502 |
| \|GAP\| | 5.9878 | 6.0047 | 5.9984 | 5.8308 |
| Descriptors (eV) | | | | |
| $\chi$ | -2,9939 | -3,0024 | -2,9992 | 3.466 |
| $\mu$ | -2,8765 | -2,9924 | -2,9747 | -3.466 |
| $\eta$ | 2,9939 | 3,0024 | 2,9992 | 2.916 |
| $S$ | 0,1670 | 0,1665 | 0,1667 | 0.343 |
| $\omega$ | 1,3819 | 1,4912 | 1,4752 | 2.060 |
| $E$ | -8,6120 | -8,9841 | -8,9217 | |

| B3LYP/6-31G* method | | | | | |
|---|---|---|---|---|---|
| Frontier orbitals (eV) | Thione[c] | Thiol[c] | Thymidine[d] | CN[-e] | Saxitoxin[e] |
| HOMO | -6.4443 | -6.8847 | -6.9621 | -21.0491 | -13.656 |
| LUMO | -2.7918 | -2.6194 | -1.4443 | -18.8917 | -7.1273 |
| GAP | -3.6525 | -4.2653 | -5.5178 | -2.1574 | -6.5287 |
| Descriptors (eV) | | | | | |
| $\chi$ | -1.8263 | -2.1327 | -2.7589 | -1.0787 | -3.2644 |
| $\mu$ | -4.61805 | -4.7521 | -4.2032 | -19.9704 | -10.3917 |
| $\eta$ | 1.8263 | 2.1327 | 2.7589 | 1.0787 | 3.2644 |
| $S$ | 0.2738 | 0.2345 | 0.1812 | 0.4635 | 0.1532 |
| $\omega$ | 5.8388 | 5.2943 | 3.2018 | 184.8600 | 16.5403 |
| $E$ | -8.4337 | -10.1345 | -11.5962 | -21.5421 | -33.9220 |

$\chi$ = - [E(LUMO) - E(HOMO)]/2; $\mu$ = [E(LUMO) + E(HOMO)]/2; $\eta$ = [E(LUMO) − E(HOMO)]/2;

$S$ = ½$\eta$; $\omega$ = $\mu^2/2\eta$; E=$\mu*\eta$, [a]This work, [b]From Ref [12], [c]From Ref [32], [d]From Ref [33], [e]From Ref [28]

Evaluating the values presented in Table 7 we observed that the frontier orbitals for the three isomers do not present greater variations, hence, *C2* and *C1* are the less and most reactive, respectively while *C3* presents a reactivity practically similar to *C2*. When these values are compared with that reported for MTX by using the 6-311++G** basis set a reduction in the reactivity value it is observed. Comparing the values of the descriptors for the three isomers, we observed notable differences among them, especially in the values of *C1*, thus, this isomer presents <$\chi$, $\mu$, $\eta$, $\omega$and E but high value of *S*, because it presents slightly higher reactivity. On the other side, the values for *C2* and *C3* are very similar to them. Later, probably the properties that present MTX could be easily attributed to the presence of the *C1*isomer in the solid state, as observed experimentally (remember, *C2* correspond to the B form while *C1* to the A form). When these descriptors are compared with those reported for the two antimicrobial tautomers of 1,3-benzothiazole, thione and thiol [32], the antiviral thymidine [33] and with those toxic species as CN^{-} and saxitoxin [28], we observed for the three isomers of MTX values of electrophilicity index closer to thymidine [33] while they have nucleophilicity index nearer to thione [32]. Thus, these results support clearly the biological properties of MTX because their three isomers have reactivities and behaviors similar to those values reported for thione [32] and thymidine [33].

## 4. Vibrational analysis

Here, only the *C1* and *C2* isomers were considered in this analysis because the *C1* isomer corresponds to the experimental polymorphic form A while *C2* to the form B [4], as was analyzed in section 3.1 and, as was shown in Figure 3. In**Figures 5** and **6** can be seen the infrared and Raman predicted for *C1* compared with the corresponding experimental ones taken from Refs [1,3] while in **Figures 7** and **8** are shown the infrared and Raman predicted for *C2* compared with the corresponding experimental ones taken from Refs [1,3]. Here, better correlations can be observed in the Raman spectra of both isomers because the predicted Raman spectra for these isomers expressed in activities were converted to intensities, as suggested in the literature by some authors [38,39]. A total de 87 vibration

*Citation: Silvia Antonia Brandán et al. Ijsrm.Human, 2018; Vol. 8 (3): 312-334.*

324

normal modes is expected for both isomers and, where all these modes present activities in both IR and Raman spectra.
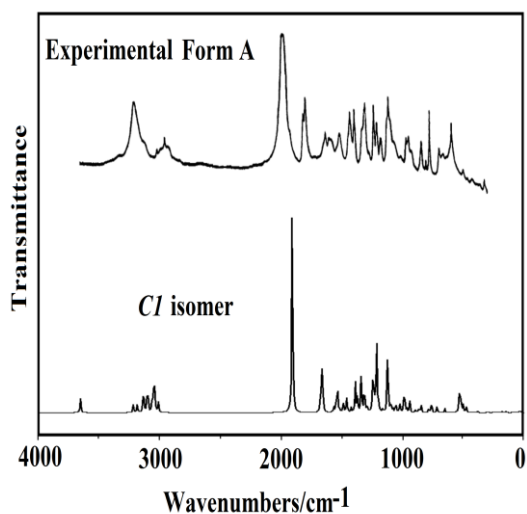


**Figure 5. Predicted infrared spectrum for the *C1* isomer compared with the corresponding experimental from Ref. [1].**
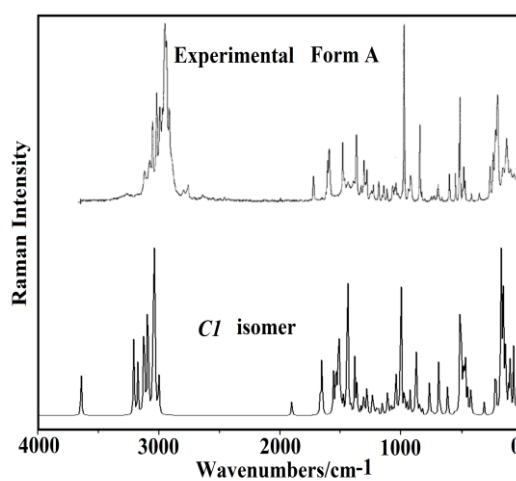


**Figure 6. Predicted Raman spectrum for the *C1* isomer compared with the corresponding experimental from Ref. [3].**
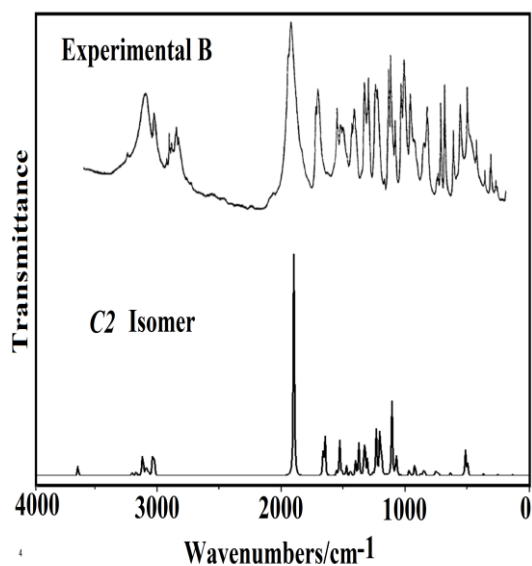


**Figure 7**. **Predicted infrared spectrum for the *C2* isomer compared with the corresponding experimental from Ref. [1].**
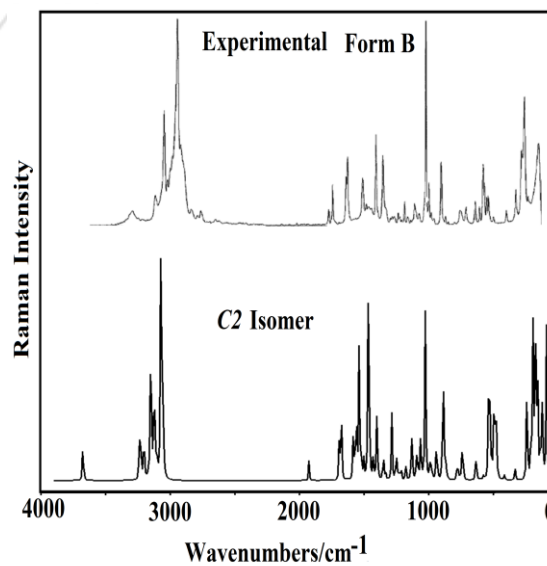


**Figure 8**. **Predicted Raman spectrum for the *C2* isomer compared with the corresponding experimental from Ref. [3].**

*Citation: Silvia Antonia Brandán et al. Ijsrm.Human, 2018; Vol. 8 (3): 312-334.*

325

The harmonic force fields for both isomers were calculated by using the SQMFF methodology [18], their normal internal coordinates and the Molvib program [19]. Here, the scale factors reported in the literature for the B3LYP/6-31G* method was used in the refinement process [18]. The vibrational assignments for both isomers were performed considering the potential energy distribution (PED) contributions ≥ 10%. Later, the observed and calculated wavenumbers are presented in **Table 8** together with the corresponding assignments for C1 and C2 in the gas phase by using the B3LYP/6-31G* level of theory. The bands located in the experimental IR spectra of both isomerscorresponding to the polymorphic forms A and B at 3270/3260, 1133-1127, 972/968 and 121/112 cm$^{-1}$ could probably be attributed to dimeric species of both isomers because these species were experimentally observed in the solid phase state by Aitipamula et al. [4]. Later, the assignments performed for some groups are presented below.

**Table 8. Observed and calculated wavenumbers (cm$^{-1}$) and assignments for two isomers of 5-[(3,5-dimethylphenoxy)methyl]-1,3-oxazolidin-2-one.**

| Experimental | | Form A | | | *C1*[a] | Form B | | | *C2*[a] |
|---|---|---|---|---|---|---|---|---|---|
| IR[c] | Ra[c] | IR[d] | Ra[e] | SQM[b] | Assignment[a] | IR[d] | Ra[e] | SQM[b] | Assignment[a] |
| 3465 | 3485 | 3437 | | 3491 | νN4-H22 | 3478w | | 3495 | νN4-H22 |
| | | 3256 | 3233w | | Dimer? | 3266s | 3266w | | Dimer? |
| 3073 | 3083 | | 3090 | 3075 | νC10-H23 | | | 3078 | νC10-H23 |
| 3049 | 3056 | 3122s | 3046 | 3074 | νC11-H24 | 3158m | 3090w | 3070 | νC11-H24 |
| 3013 | 3018 | | 3022 | 3044 | νC14-H25 | 3007w | 3019s | 3045 | νC14-H25 |
| | 2990 | | 2988m | 2999 | νₐCH₃(C16) | | 2995w | 2998 | νₐCH₃(C16) |
| | | | | 2997 | νₐCH₃(C15) | | | 2998 | νₐCH₃(C15) |
| | | 2981 | | 2990 | νC5-H17 | | | 2994 | νC5-H17 |
| | 2965 | | 2961 | 2967 | νₐCH₃(C16) | 2977m | 2971sh | 2987 | νₐCH₂(C6) |
| | | | | 2964 | νₐCH₃(C15) | | | 2968 | νₐCH₃(C16) |
| | 2952 | | 2940 | 2958 | νₐCH₂(C6) | 2949w | 2953sh | 2966 | νₐCH₃(C15) |
| | | 2931 | | 2928 | νₐCH₂(C7) | | | 2950 | νₐCH₂(C7) |
| | | | 2919vs | 2918 | νₛCH₃(C16) | | 2920vs | 2918 | νₛCH₃(C16) |
| 2916 | 2916 | | | 2916 | νₛCH₃(C15) | | | 2917 | νₛCH₃(C15) |
| 2887 | | 2889 | 2908 | 2906 | νₛCH₂(C6) | 2891m | 2894sh | 2908 | νₛCH₂(C6) |
| | | 2837 | 2885m | 2878 | νₛCH₂(C7) | 2863sh | 2810w | 2904 | νₛCH₂(C7) |
| 1737 | 1784 | 1742v | 1725m | 1832 | νC8=O3 | 1784vs | 1746m | 1833 | νC8=O3 |
| | 1641 | 1613s | 1612m | 1614 | νC12-C14 | 1616s | 1716m | 1613 | νC12-C14 |
| | | h | | | νC9-C11 | | | | νC9-C11 |
| 1609 | | 1600s | 1596m | 1600 | νC9-C10 | 1616s | 1606s | 1600 | νC9-C10 |
| | 1512 | | | 1492 | δCH₂(C6) | 1493m | | 1492 | δCH₂(C6) |
| | | | 1486m | 1484 | δₐCH₃(C16) | | 1486m | 1485 | δCH₂(C7) |
| | | | | | δCH₂(C7) | | | | δₐCH₃(C16) |
| | 1481 | 1474 | 1470w | 1477 | δₐCH₃(C15) | 1472m | 1478sh | 1477 | δₐCH₃(C15) |
| | | | 1462sh | 1464 | δCH₂(C7) | 1457m | 1458w | 1472 | δCH₂(C7) |
| 1452 | 1454 | 1450 | 1450sh | 1450 | δₐCH₃(C16) | | | 1450 | δₐCH₃(C15) |
| | | | | 1450 | δₐCH₃(C15) | | | 1449 | δₐCH₃(C16) |

*Citation: Silvia Antonia Brandán et al. Ijsrm.Human, 2018; Vol. 8 (3): 312-334.*

326

| | | | | | Assignment | | | | Assignment |
|---|---|---|---|---|---|---|---|---|---|
| | | | 1444w | 1446 | $\delta_a CH_3(C16)$ | | | 1446 | $\delta_a CH_3(C16)$ |
| 1433 | 1433 | | 1434sh | 1427 | $\delta_a CH_3(C15)$ | 1439sh | 1440w | 1426 | $\delta_a CH_3(C15)$ |
| | | | | | $wag CH_2(C7)$ | | | | $\delta_a CH_3(C16)$ |
| | 1424 | | | 1422 | $wag CH_2(C6)$ | 1411sh | 1416w | 1415 | $wag CH_2(C6)$ |
| | | | | | | | | | $\beta N4\text{-}H22$ |
| | | | 1419w | 1419 | $wag CH_2(C7)$ | 1399m | | 1411 | $wag CH_2(C7)$ |
| 1387 | | 1384 | 1397w | 1381 | $\rho' C5\text{-}H17$ | 1387m | 1382s | 1380 | $\delta_s CH_3(C15)$ |
| | 1379 | | 1374s | 1379 | $\delta_s CH_3(C16)$ | | | 1377 | $\delta_s CH_3(C16)$ |
| | | 1369s | 1367sh | 1377 | $\delta_s CH_3(C15)$ | | | 1371 | $\rho C5\text{-}H17$ |
| | | 1328s | 1337w | 1337 | $\beta N4\text{-}H22$ | | 1340sh | 1338 | $\rho' C5\text{-}H17$ |
| 1324 | 1327 | 1318 | 1312m | 1334 | $\nu C11\text{-}C13$ | 1323s | 1328s | 1332 | $\nu C11\text{-}C13$ |
| 1296 | 1299 | 1294 | 1299w | 1299 | $\beta C14\text{-}H25$ | 1297s | 1306sh | 1298 | $\beta C14\text{-}H25$ |
| | | 1285s | 1290m | 1282 | $\rho C5\text{-}H17$ | 1297s | | 1297 | $wag CH_2(C6)$ |
| | | h | | | | | | | $\rho' C5\text{-}H17$ |
| 1251 | 1263 | | 1259sh | 1269 | $\nu C14\text{-}C13$ | 1255s | 1262w | 1269 | $\nu C14\text{-}C13$ |
| 1232 | 1236 | 1228s | 1234w | 1253 | $\rho CH_2(C7)$ | 1243s | | 1232 | $\rho CH_2(C7)$ |
| | | 1204s | 1191m | 1205 | $\nu C8\text{-}N4$ | 1243s | 1208w | 1203 | $\nu C8\text{-}N4$ |
| 1178 | 1195 | 1172 | 1163sh | 1194 | $\rho CH_2(C6)$ | 1199w | 1197w | 1182 | $\rho CH_2(C6)$ |
| 1158 | 1159 | 1151 | | 1170 | $\beta C10\text{-}H23$ | 1172s | | 1167 | $\beta C10\text{-}H23$ |
| | | w | | | $\nu C9\text{-}O2$ | | | | $\nu C9\text{-}O2$ |
| | | | 1149w | 1157 | $\beta C11\text{-}H24$ | 1159s | 1157m | 1156 | $\beta C11\text{-}H24$ |
| 1135 | 1131 | 1127 | 1121w | | Dimer? | 1130m | 1133w | | Dimer? |
| 1093 | 1095 | 1087s | 1079w | 1089 | $\nu C5\text{-}C7$ | | | 1092 | $\nu C5\text{-}C7$ |
| 1082 | 1080 | 1081 | | 1081 | $\nu C7\text{-}O2$ | 1094s | 1081w | 1075 | $\nu C7\text{-}O2$ |
| | | 1068s | 1061w | 1070 | $\nu C6\text{-}N4$ | 1076s | 1068sh | 1065 | $\nu C6\text{-}N4$ |
| | | 1052s | 1050w | 1049 | $\rho CH_3(C16)$ | | | 1049 | $\rho CH_3(C15)$ |
| | 1048 | | | 1048 | $\rho CH_3(C15)$ | | 1046w | 1048 | $\rho CH_3(C16)$ |
| | | | 1036sh | 1041 | $\nu C5\text{-}O1$ | 1035m | 1036sh | 1037 | $\nu C5\text{-}O1$ |
| | | | | | $\tau w CH_2(C7)$ | 1035m | 1036sh | 1023 | $\tau w CH_2(C7)$ |
| | | | | 1021 | $\rho' CH_3(C15)$ | | 1014sh | 1020 | $\rho' CH_3(C15)$ |
| 1011 | | 1000 | | 1017 | $\rho' CH_3(C16)$ | 1014sh | 1004sh | 1007 | $\rho' CH_3(C16)$ |
| 994 | 994 | | 984vs | 990 | $\beta R_1(A6)$ | 994sh | 996vs | 990 | $\beta R_1(A6)$ |
| | | 968m | | 977 | $\nu C5\text{-}C6$ | | 972m | | Dimer? |
| | | 952m | 948w | 943 | $\nu C12\text{-}C15$ | 950sh | | 944 | $\nu C12\text{-}C15$ |
| 932 | 933 | | 930m | 930 | $\nu C13\text{-}C16$ | 930m | | 933 | $\nu C13\text{-}C16$ |
| | | 917sh | 919sh | 923 | $\nu C8\text{-}O1$ | 914sh | | 902 | $\nu C8\text{-}O1$ |
| | | 872w | | 885 | $\tau w CH_2(C6)$ | | 880s | 890 | $\tau w CH_2(C6)$ |
| 876 | 877 | | 861sh | 876 | $\gamma C11\text{-}H24$ | 865w | | 874 | $\gamma C14\text{-}H25$ |
| | | | 855s | 856 | $\tau w CH_2(C6)$ | | | 851 | $\gamma C11\text{-}H24$ |
| 846 | 843 | 844w | 838w | 851 | $\gamma C14\text{-}H25$ | 844m | 841w | 844 | $\gamma C10\text{-}H23$ |
| 825 | 822 | 820s | 815vw | 832 | $\gamma C10\text{-}H23$ | 818s | 821w | 832 | $\gamma C11\text{-}H24$; $\gamma C10\text{-}H23$ |
| | | | | | | | | | $\nu C5\text{-}C6$ |
| 740 | 754 | 761w | 761w | 767 | $\beta R_1(A5)$ | 766m | 775w | 757 | $\beta R_1(A5)$ |
| | 726 | 736w | 739w | 746 | $\gamma C8\text{-}O3$ | 721m | | 745 | $\gamma C8\text{-}O3$ |
| 717 | | | 708m | 695 | $\beta R_2(A5)$ | | 727w | 725 | $\beta R_2(A5)$ |
| 687 | 683 | 686m | 672w | 681 | $\tau R_1 (A6)$ | 678s | 684w | 682 | $\tau R_1 (A6)$ |
| 611 | 612 | 611w | 616m | 632 | $\delta C7O2C9$ | 621w | 612w | 627 | $\delta C7O2C9$ |
| 579 | 581 | 583w | | 579 | $\gamma C9{=}O2$ | 568w | 582w | 578 | $\gamma C9{=}O2$ |

*Citation: Silvia Antonia Brandán et al. Ijsrm.Human, 2018; Vol. 8 (3): 312-334.*

327

| | | | | | Assignment | | | | Assignment |
|---|---|---|---|---|---|---|---|---|---|
| | | 554w | 562m | 538 | βR₃(A6) | | 552s | 540 | βC9=O2 |
| 545 | 550 | | 533sh | 531 | βC9=O2 | 535sh | 542sh | 535 | βR₃(A6) |
| 526 | 522 | | 529vs | 521 | γC13-C16 | 530w | 522sh | 520 | τR₂(A6) |
| | 509 | 508w | 500sh | 519 | γC12-C15 γN4-H22 | | 517w | 512 | γC12-C15 γN4-H22 |
| 495 | 508 | | 496m | 507 | δO3C8O1 βR₂(A6) | 497w | 498sh | 506 | βR₂(A6) |
| 474 | 477 | 479w | 484w | 490 | γN4-H22 | 492sh | 472w | 491 | γN4-H22 |
| 459 | | | 431w | 463 | δO2C8O1 δC7C5O1 | 453w | | 439 | δO2C8O1 δC7C5O1 |
| 371 | | | 367w | 371 | δC7C5C6 βC13-C16 | | 370w | 366 | δC7C5C6 |
| 297 | | | 280m | 289 | βC12-C15 βC12-C15 | | 300m | 288 | βC12-C15 |
| | | | 254m | 245 | βC13-C16 | | 254sh | 257 | βC13-C16 |
| 232 | | | 232s | 239 | τR₂ (A6) | | 231vs | 238 | τR₂ (A6) |
| | | | 222sh | 224 | τR₃ (A6) | | 224sh | 224 | τR₃ (A6) |
| 201 | | | 218vs | 210 | δC5C7O2 | | 217sh | 210 | δC5C7O2 |
| | | | 176m | 184 | τR₁ (A5) τR₂ (A6) | | 200w | 184 | τR₂ (A6) |
| | | | 157sh | 168 | τR₁ (A6) τR₁ (A5) | | 164sh | 166 | τR₁ (A6) τR₁ (A5) |
| | | | 144s | 134 | τR₂ (A5) | | 132sh | 132 | τwC7-C5 |
| 118 | | | 112m | | τwC7-C5 Dimer? | | 121s | | Dimer? |
| | | | 84w | 82 | δC5C7O2 | | 114sh | 94 | τwC7-C5 |
| 73 | | | | 67 | τwO2-C9 τR₂ (A5) | | | 53 | τwO2-C9 τR₂ (A5) |
| | | | | 45 | C7-C5 τwCH₃(C15) | | | 40 | τwCH₃(C15) |
| | | | | 34 | τwCH₃(C16) | | | 30 | τC7-O2 |
| | | | | 28 | τC7-O2 | | | 23 | τwO2-C9 |
| | | | | 21 | τwO2-C9 | | | 19 | τwCH₃(C16) |
| | | | | | | | | | γC13-C16 |

Abbreviations: ν, stretching; wag, wagging; τ, torsion; ρ, rocking; τw, twisting; δ, deformation; a, antisymmetric; s, symmetric; [a]This work; [b]From scaled quantum mechanics force field B3LYP/6-31G* method; [c]From Ref [12]; [d]From Ref [1]; [e]From Ref [3]

### 4.1. BandAssignments

**4.1.1. N-H modes**. In the anti-hypertensive clonidine hydrochloride agent, the NH stretching modes [40] were assigned to the bands between 3427 and 3341 cm$^{-1}$ while when these groups are involved in the H bonds (dimer) they are assigned in approximately 2584 cm$^{-1}$. Hence, the two IR bands observed in the experimental IR spectra of both isomers A and B of MTX at 3478/3437 cm$^{-1}$ and those bands observed in the 3270-3260 cm$^{-1}$ region can also be assigned

*Citation: Silvia Antonia Brandán et al. Ijsrm.Human, 2018; Vol. 8 (3): 312-334.*

328

to these vibration modes while the group of IR bands between 2716-2322 cm$^{-1}$ that in the Raman spectra appear between 2761-2434 cm$^{-1}$ could be attributed to the H bonds due to the dimeric species of A and B, as observed experimentally by Aitipamula et al. [4]. The N-H in-plane deformation modes for *C1* and *C2* are predicted by SQM calculations in different regions, thus, in *C1* is predicted in 1337 cm$^{-1}$ while in *C2* at 1415 cm$^{-1}$. Then, they were assigned in these regions. The corresponding N-H out-of-plane deformation modes are predicted in both isomers in the same regions and coupled with other deformation modes, hence, they were assigned between 519-472 cm$^{-1}$.

**4.2.1. C-H modes**. For both isomers are expected four C-H stretching modes where three of them correspond to CH groups with C atoms in sp$^2$ hybridizations while the remains C5-H17 groups belong to a C atom with sp$^3$ hybridization. This way, the three C10-H23, C11-H24 and C14-H25 stretching modes are assigned to higher wavenumbers than the other ones, as predicted by SQM calculations and, as observed in Table 8. Here, obviously, the in-plane and out-of-plane deformation modes only are expected for the CH groups with sp$^2$ hybridizations while for the C5-H17 groups of both isomers are expected two rocking and deformation modes, as indicated in Table 8. Thus, the in-plane and out-of-plane deformation modes corresponding to the C1-H25, C3-H7 and C4-H6 groups are assigned to the bands observed in the 1229/1156 and 876/832 cm$^{-1}$ regions, respectively, as predicted by calculations. Note that the two rocking modes for the C5-H17 groups are predicted in *C1* at 1381 and 1282 cm$^{-1}$ while in *C2* these modes are predicted at 1371 and 1338 cm$^{-1}$. Hence, the IR and Raman bands observed in these regions are assigned to these vibration modes.

**4.3.1. CH$_3$ modes.** For these groups, due to the presence of two CH$_3$ groups in both isomers of MTX, a total of 18 vibration normal modes are expected. Hence, the antisymmetric and symmetric modes are associated to the IR and Raman bands between 2999 and 2916 cm$^{-1}$ where clearly the symmetric modes of *C1* and *C2* are assigned to the very intense Raman bands at 2919 and 2920 cm$^{-1}$, respectively. The corresponding deformation modes are predicted between 1485 and 1377 cm$^{-1}$, as observed in species containing these groups [27,29,30,33]. The rocking modes in both isomers are predicted between 1049 and 1007 cm$^{-1}$ and, for this reason, they are assigned to the bands observed in this region. The twisting modes in species containing these groups are predicted in the lower wavenumbers [27,29,30,33], here, these modes are predicted between 45 and 20 cm$^{-1}$, as indicated in Table 8.

*Citation: Silvia Antonia Brandán et al. Ijsrm.Human, 2018; Vol. 8 (3): 312-334.*

329

**4.4.1. CH$_2$ modes**. Here, the antisymmetric and symmetric stretching modes expected for both isomers are predicted by SQM calculations between 2958 and 2878 cm$^{-1}$, hence, these modes were assigned to the IR and Raman bands observed in that region. The deformation, wagging, rocking and twisting modes expected for both isomers are predicted by calculations in the 1485/1472, 1422/1297, 1253/1182 and 1041/885 cm$^{-1}$ regions, respectively. Accordingly, the IR and Raman bands observed in these regions were assigned to those vibration modes.

**4.5.1. Skeletal modes.** The C8=O3 stretching modes in both isomers can be easily assigned to the very strong IR bands at 1742/1784 cm$^{-1}$ while the C=C stretching modes belonging to the six members rings in both isomers are predicted in different regions, thus, the C10-C12 and C9-C10 and C9- C11 stretching modes are predicted at higher wavenumbers than the C11-C13 and C13-C14 stretching modes, hence, these latter two bonds show partial double bonds characters. Here, in both isomers, it is observed that the C5-O1 stretching modes belonging to the oxazolidinone rings are predicted at higher wavenumbers than the other C8-O1 stretching modes. Evidently, the C8=O3 stretching has notable influence on the frequencies of the C8-O1 stretching modes. On the other hand, the two N4-C6 and N4-C8 stretching modes are predicted in both isomers in the same regions, hence, they are assigned as predicted by calculations and, as shown in Table 8. The two C-CH$_3$ stretching modes (C12-C15 and C13-C16) of both isomers were predicted in the same regions and, this way, these modes are assigned to the bands between 952 and 930 cm$^{-1}$. Note that the C5-C6 stretching modes that also belong to the oxazolidinone rings are predicted in different regions, thus, in *C1* it is predicted at 977 cm$^{-1}$ while in *C2* at 932 cm$^{-1}$ coupled with a CH out-of-phase deformation mode. This observation could also be justified by the different MK charges for the C5 and C6 atoms. Probably, these different properties also explain why the two expected deformations β$_{R1}$ and β$_{R2}$ and two torsions τ$_{R1}$ and τ$_{R2}$ rings, for the oxazolidinone rings in both isomers are predicted in different regions while for the ring of six members in the two isomers are predicted in the same regions and, as reported for similar species [27,29-31,33,40].

## 4. Force constants

For the two isomers of MTX were calculated the harmonic force constants from the corresponding harmonic force fields calculated by the using 6-31G* level of theory with the

*Citation: Silvia Antonia Brandán et al. Ijsrm.Human, 2018; Vol. 8 (3): 312-334.*

330

SQMFF methodology [18] and the Molvib program [19]. The results are summarized in **Table 9**.

**Table 9. Comparison of scaled internal force constants for the two isomers of 5-[(3,5-dimethylphenoxy)methyl]-1,3-oxazolidin-2-one in the gas phase.**

| B3LYP6-31G* Method[a] | | |
|---|---|---|
| Force constants | *C1* | *C2* |
| $f(\nu C=O)$ | 12.76 | 12.74 |
| $f(\nu C\text{-}O)_{R5}$ | 4.65 | 4.61 |
| $f(\nu C\text{-}O)$ | 5.39 | 5.31 |
| $f(\nu C\text{-}N)$ | 5.44 | 5.47 |
| $f(\nu N\text{-}H)$ | 6.75 | 6.77 |
| $f(\nu C\text{-}H)_{R6}$ | 5.16 | 5.16 |
| $f(\nu CH_2)$ | 4.69 | 4.76 |
| $f(\nu CH_3)$ | 4.84 | 4.84 |
| $f(\nu C=C)$ | 6.45 | 6.45 |
| $f(\nu C\text{-}C)_{R5}$ | 3.88 | 3.95 |
| $f(\delta CH_2)$ | 0.80 | 0.80 |
| $f(\delta CH_3)$ | 0.55 | 0.55 |

Units are mdyn $\text{Å}^{-1}$ for stretching and mdyn $\text{Å rad}^{-2}$ for angle deformations

[a]This work

The results for *C1* and *C2* show slight differences in some constants especially in those related to the oxazolidinone rings, as compared with the corresponding to the dimethylphenoxy-methyl rings. Thus, the higher differences can be observed in the $f(\nu C\text{-}C)_{R5}$ force constants which are directly related to the C5-C6 bonds where both atoms of the two isomers have shown different MK charges values, as observed in Table 3. The force constants values related to the dimethylphenoxy-methyl rings are practically similar in both isomers including those constants related to the CH$_3$ groups. The harmonic force constants values for *C1* and *C2* show values comparable to those reported for molecules with similar groups [28-33,40].

*Citation: Silvia Antonia Brandán et al. Ijsrm.Human, 2018; Vol. 8 (3): 312-334.*

331

## 5. CONCLUSIONS

Here, we have performed a theoretical study on the muscle relaxant 5-[(3,5-dimethylphenoxy)methyl]-1,3-oxazolidin-2-one, of generic name metaxolone, by using the hybrid B3LYP/6-31G* calculations in the gas phase. Three isomers (*C1,* C2, and *C3*) were found in the PES but only two of them named *C1* and *C2* correspond to the two experimentally reported polymorphic forms A and B, respectively. The high values in the dihedral C5-C7-O2-C9 and O1-C5-C7-O2 angles, different from the experimental ones, probably support the absence of *C3* isomer in the solid phase. However, the higher bond orders values together with the high topological properties observed for the oxazolidinone ring of *C1* could possibly support their existence despite this isomer has the highest energy than *C2* and *C3*. The NBO analyses reveal the high stabilities of *C1* and *C2* while the AIM study suggests that the ring dimethylphenoxy-methyl practically do not have influence on the properties of metaxolone. The frontier orbitals show that the isomers of metaxolone have reactivities and electrophilicity indexes similar to antiviral thymidine while their nucleophilicity indexes are closer to antimicrobial thione. On the other hand, the complete vibrational assignments of those two structures were performed by using the experimental available FT-IR and FT-Raman spectra, their normal internal coordinates, the SQMFF methodology and the Molvib program. The harmonic force fields for the two isomers and their force constants were also reported.

## REFERENCES

[1] Chattopadhyay et al., Metaxolone Polymorphs, Patent US 2007/0185177 A1, 2007.

[2] Toth PE, Urtis J. Commonly used muscle relaxant therapies for acute low back pain: a review of carisoprodol, cyclobenzaprine hydrochloride, and metaxolone, Clinical Therapeutics. 2004, 26(9): 1355–1367,.

[3] Lorimer et al. Patent, Amorphous metaxolone and amorphous dispersions thereof, US 2009/0163561 A1, 2009.

[4] Aitipamula S, Chow PS, Tan RBH, Conformational Polymorphs of a Muscle Relaxant, Metaxolone, *Cryst. Growth Des.*2011, 11 (9): 4101–4109.

[5] Lin H, Wu T, Huang Y, Lin S. Studies on Cocrystal Formation of Metaxolone with Short-chain Dicarboxylic Acids, Acta Cryst.(2014), A70: C658.

[6] Sumadeepthi B, Nagaraju G, Ramakotaiah M, Rao MP. In-Vitro evaluation of newly formulated metaxolone tablets for immediate release by wet granulation technique, IJIPSR 2014, 2(10): 2425-2437.

*Citation: Silvia Antonia Brandán et al. Ijsrm.Human, 2018; Vol. 8 (3): 312-334.*

332

[7] Prasad PR, Bhuvaneswari K, Murarilal, Rajani K, Sunanda B. Determination of metaxolone and diclofenac potassium in combined dosage form by FT-IR spectroscopy, International Journal of Biological & Pharmaceutical Research. 2015, 6(2): 155-160.

[8] Chintan R Patel, Ritu V Kimbahune, Prachi V Kabra, Harish AR, Nargund LVG, Spectrophotometric Estimation of Metaxolone and Diclofenac Potassium by Multicomponent Analytical Method from Tablet Dosage Form, J Anal Bioanal Techniques 2012, 3(3): 1-3.

[9] Lin H-L, Chi Y-T, Huang Y-T, Kao C-Y, Lin S-Y. DSC-FTIR Combined Approaches Used to Simultaneously Prepare/Determine the Amorphous Solid Dispersions of Indomethacin/Soluplus in Real-time, EC Pharmaceutical Science2015, 2(1): 183-193.

[10] Hong M, Wu S, Qi M, Ren G, Solubility correlation and thermodynamic analysis of two forms of Metaxolone in different pure solvents, Fluid Phase Equilibria 2016, 40: 1-6.

[11] Gubbala LP, Arutla S, Venkateshwarlu V. Optimization of Composition and Process for Preparing Metaxolone Nanosuspension using Factorial Design, International Journal of Drug Delivery Technology 2016, 6(3): 79-91.

[12] Boopathi M, Udhayakala P, Ramkumar GR. Vibrational spectroscopic (FT-IR, FT-Raman), NMR and electronic structure calculations of metaxolone, Der Pharma Chemica, 2016, 8(7):161-172.

[13] Poklis JL, Ropero-Miller JD, Garside D, Winecker RE, Metaxolone (Skelaxin)-related deathJ Anal Toxicol. 2004, 28(6):537-41.

[14] Bishop-Freeman SC, et al. Postmortem Metaxolone (Skelaxin®) Data from North Carolina, J Anal Toxicol 2015; 39(8):629-36.

[15] Martini DI, Nacca N, Haswell D, Cobb T, Hodgman M. Serotonin syndrome following metaxolone overdose and therapeutic use of a selective serotonin reuptake inhibitor, Clin Toxicol (Phila). 2015, 53(3):185-7.

[16] Dipak Dilip Gadade, Sanjay Sudhakar Pekamwar, Pharmaceutical Cocrystals: Regulatory and Strategic Aspects, Design and Development, Adv Pharm Bull, 2016, 6(4): 479-494.

[17] Lin SY. Simultaneous screening and detection of pharmaceutical co-crystals by the one-step DSC–FTIR microspectroscopic technique, Drug Discovery Today, 2017, 22(4): 718-728.

[18] a) Rauhut G, Pulay P. J. Phys. Chem. 1995, 99: 3093-3099. b) *Correction:* Rauhut G, Pulay P. J. Phys. Chem. 1995, 14572.

[19] Sundius T. Scaling of ab-initio force fields by MOLVIB. Vib. Spectrosc. 2002; 29:89-95.

[20] Becke AD. Density functional thermochemistry. III. The role of exact exchangeJ. Chem. Phys. 1993, 98:5648-5652.

[21] Lee C, Yang W, Parr RG. Development of the Colle-Salvetti correlation-energy formula into a functional of the electron density, Phys. Rev. 1988, B37: 785-789.

[22] Glendening ED, Badenhoop JK, Reed AD, Carpenter JE, Weinhold F. 1996. NBO 3.1; Theoretical Chemistry Institute, University of Wisconsin; Madison.

[23] Biegler-Köning F, Schönbohm J, Bayles DJ. AIM2000; a program to analyze and visualize atoms in molecules. Comput. Chem. 2001; 22:545-559.

[24] Bader RFW. Atoms in Molecules, A Quantum Theory, Oxford University Press, Oxford, ISBN: 0198558651, 1990.

[25] Parr RG, Pearson RG. Absolute Hardness: companion parameter to absolute electronegativity. J. Am. Chem. Soc. 1983; 105:7512-7516.

[26] Brédas J-L. Mind the gap!. Materials Horizons 2014; 1:17–19.

[27] Romani D, Márquez MJ, Márquez MB, Brandán SA. Structural, topological and vibrational properties of an isothiazole derivatives series with antiviral activities. J. Mol. Struct. 2015; 1100:279-289.

[28] Romani D, Tsuchiya S, Yotsu-Yamashita M, Brandán SA. Spectroscopic and structural investigation on intermediates species structurally associated to the tricyclic bisguanidine compound and to the toxic agent, saxitoxin, J. Mol. Struct. 2016, 1119: 25-38.

[29] Chain F, Iramain MA, Grau A, Catalán CAN, Brandán SA. Evaluation of the structural, electronic, topological and vibrational properties of *N*-(3,4-dimethoxybenzyl)-hexadecanamide isolated from Maca (*Lepidium meyenii*) using different spectroscopic techniques, J. Mol. Struct. 2016, 1119: 25-38.

*Citation: Silvia Antonia Brandán et al. Ijsrm.Human, 2018; Vol. 8 (3): 312-334.*

333

[30] Chain FE, Ladetto MF, Grau A, Catalán CAN, Brandán SA. Structural, electronic, topological and vibrational properties of a series of N-benzylamides derived from Maca (Lepidium meyenii) combining spectroscopic studies with ONION calculations, J. Mol. Struct. 2016, 1105: 403-414.

[31] Gatfaoui S, Issaoui N, Brandán SA, Roisnel T, Marouani H. Synthesis and characterization of p-xylylenediaminiumbis(nitrate). Effects of the coordination modes of nitrate groups on their structural and vibrational properties, J. Mol. Struct. 2018, 1151: 152-168.

[32] Romani D, Brandán SA. Structural and spectroscopic studies of two 1,3-benzothiazole tautomers with potential antimicrobial activity in different media. Prediction of their reactivities. Computational and Theoretical Chem. 2015; 1061:89-99.

[33] Márquez MB, Brandán SA. A structural and vibrational investigation on the antiviral deoxyribonucleoside thymidine agent in gas and aqueous solution phases. International J. of Quantum Chem. 2014; 114(3): 209-221.

[34] Nielsen AB, Holder AJ. 2008. *GaussView* 5.0, User's Reference, GAUSSIAN Inc., Pittsburgh, PA.

[35] Gaussian 09, Revision D.01, Frisch, M. J.; Trucks, G. W.; Schlegel, H. B.; Scuseria, G. E.; Robb, M. A.; Cheeseman, J. R.; Scalmani, G.; Barone, V.; Mennucci, B.; Petersson, G. A.; Nakatsuji, H.; Caricato, M.; Li, X.; Hratchian, H. P.; Izmaylov, A. F.; Bloino, J.; Zheng, G.; Sonnenberg, J. L.; Hada, M.; Ehara, M.; Toyota, K.; Fukuda, R.; Hasegawa, J.; Ishida, M.; Nakajima, T.; Honda, Y.; Kitao, O.; Nakai, H.; Vreven, T.; Montgomery, J. A., Jr.; Peralta, J. E.; Ogliaro, F.; Bearpark, M.; Heyd, J. J.; Brothers, E.; Kudin, K. N.; Staroverov, V. N.; Kobayashi, R.; Normand, J.; Raghavachari, K.; Rendell, A.; Burant, J. C.; Iyengar, S. S.; Tomasi, J.; Cossi, M.; Rega, N.; Millam, J. M.; Klene, M.; Knox, J. E.; Cross, J. B.; Bakken, V.; Adamo, C.; Jaramillo, J.; Gomperts, R.; Stratmann, R. E.; Yazyev, O.; Austin, A. J.; Cammi, R.; Pomelli, C.; Ochterski, J. W.; Martin, R. L.; Morokuma, K.; Zakrzewski, V. G.; Voth, G. A.; Salvador, P.; Dannenberg, J. J.; Dapprich, S.; Daniels, A. D.; Farkas, Ö.; Foresman, J. B.; Ortiz, J. V.; Cioslowski, J.; Fox, D. J. Gaussian, Inc., Wallingford CT, 2009.

[36] Besler BH, Merz Jr KM, Kollman PA. Atomic charges derived from semiempirical methods. J. Comp. Chem. 1990; 11: 431-439.

[37] Ugliengo P. MOLDRAW Program, University of Torino, Dipartimento Chimica IFM, Torino, Italy, 1998.

[38] Keresztury G, Holly S, Besenyei G, Varga J, Wang AY, Durig JR. Vibrational spectra of monothiocarbamates-II. IR and Raman spectra, vibrational assignment, conformational analysis and ab initiocalculations of S-methyl-N,N-dimethylthiocarbamateSpectrochim. Acta, 1993, 49A: 2007-2026.

[39] Michalska D, Wysokinski R. The prediction of Raman spectra of platinum(II) anticancer drugs by density functional theory, Chemical Physics Letters, 2005, 403: 211-217.

[40] Romano E, Davies L, Brandán SA. Structural properties and FTIR-Raman spectra of the anti-hypertensive clonidine hydrochloride agent and their dimeric species, J. Mol. Struct. 2017, 1133: 226-235.

*Citation: Silvia Antonia Brandán et al. Ijsrm.Human, 2018; Vol. 8 (3): 312-334.*

334